

We are IntechOpen, the world's leading publisher of Open Access books Built by scientists, for scientists

6,900

Open access books available

186,000

International authors and editors

200M

Downloads

Our authors are among the

154

Countries delivered to

TOP 1%

most cited scientists

12.2%

Contributors from top 500 universities



WEB OF SCIENCE™

Selection of our books indexed in the Book Citation Index
in Web of Science™ Core Collection (BKCI)

Interested in publishing with us?
Contact book.department@intechopen.com

Numbers displayed above are based on latest data collected.
For more information visit www.intechopen.com



Luminescence in Rare Earth Ion-Doped Oxide Compounds

Carlos Ruvalcaba Cornejo

Additional information is available at the end of the chapter

<http://dx.doi.org/10.5772/65185>

Abstract

This chapter focuses on the study on luminescent materials, which consist of oxide compounds (host material) and rare earth ions (as the activator) in the valence state, mostly 3+. The first part begins with a background study about the luminescence phenomenon, its stages, and the configurational coordinate diagram. Then, we review the notation often used for rare earth ions, such as the term symbols associated with the energy levels of the ground state. Lastly on the first part, we establish a relationship between the configurational coordinate model and the electronic transitions of such ions. The second part shows the photoluminescence results in some oxide compound materials doped with rare earth ions that have been reported in research articles with potential applications.

Keywords: rare earth, luminescence, oxides, glasses, crystals

1. Introduction

1.1. Background

Luminescence can be defined as the capability of a body to emit light when exposed to electromagnetic radiation or other means such as energy from an electron, a chemical reaction, and so on. Examples are as follows: when the body is excited by low-energy photons, often ultraviolet radiation (*photoluminescence*), by cathode rays (*cathodoluminescence*), by an electric field strength (*electroluminescence*), by X-rays (*X-rays luminescence*), and so on. The light emitted by a body (a luminescent material) appears in the visible part of the electromagnetic spectrum, but can be in the infrared (IR) or ultraviolet (UV) regions.

A first application of a luminescent material is that the photoluminescence occurs in a fluorescent lamp. Such lamp consists of a glass tube in which a low-pressure mercury discharge generates ultraviolet radiation. This material converts the UV radiation in white light. Visible

light emission processes due to thermal radiation are termed *incandescence*, and not luminescence. This distinction explains why the efficiency of conversion of electricity to light is in a fluorescent lamp considerably higher than in an incandescent lamp [1]. **Figure 1** shows an example of this situation.

In the example of **Figure 1(a)**, if a photon of 3.35 eV (≈ 370 nm of wavelength in ultraviolet part of the electromagnetic spectrum) is absorbed by the phosphor, then it might emit a photon of say 2.48 eV (≈ 500 -nm green light), which is common in Stokes' process [1].

The luminescence of *inorganic* materials is composed of the following processes: (1) absorption and excitation, (2) energy transfer, and (3) emission. Most luminescent materials consist of a so-called *host* material to which certain dopant ions, also termed *activators*, are added. In such cases, the host lattice plays two distinct roles: as a *passive matrix* to define the spatial locations of the activator ions; and as an *active participant* in the luminescence process, exerting its own specific influence on the spectroscopic behavior of the activator. In the latter, it helps to shape the structure of the energy levels of the activator and also introduces vibrations of various energies, the so-called *phonons*, which influence the kinetics of the luminescence phenomena.

Consider the luminescence phenomenon in the simple case as follows. **Figure 2(a)** shows that the exciting radiation is absorbed by the activator ion (A) into a host material. A system of two electronic states, the ground energy state (*g*) and a higher-lying "excited" level (*e*), is schematized in **Figure 2(b)**. The process of excitation, which supplies energy to the host matrix, raises

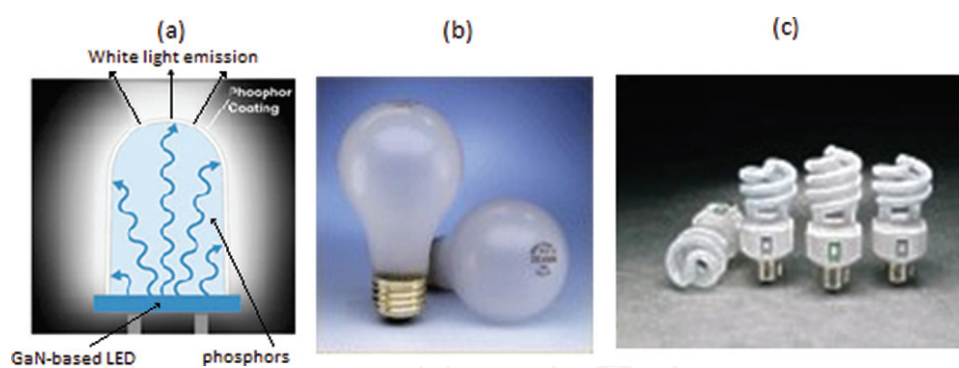


Figure 1. (a) Solid-state lighting: based on GaN blue- (400 nm) or UV- (370–400-nm) light-emitting diodes (LEDs). (b) and (c) white-light lamps: traditional designs.

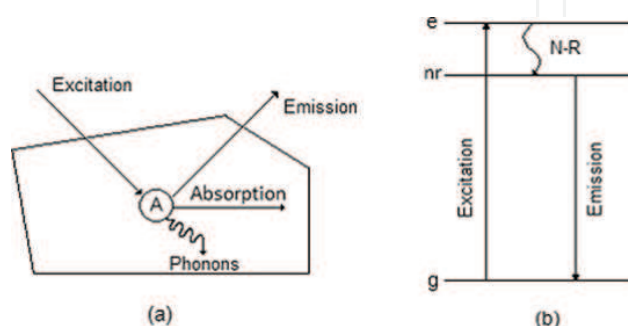


Figure 2. (a) An activator ion A in a passive host lattice and (b) schematic depiction of excitation (absorption) and emission processes in an activator A.

an electron from the g state to the e level. Most of the excitation energy moves to a different lower-lying state, with the remainder being dissipated without emission of light, through the so-called *non-radiative* (N-R) *relaxation*, $e \rightarrow (nr)$. This configuration then relaxes to the ground state by sending off a photon of light, a *radiative emission* $(nr) \rightarrow g$. This completes the process, allowing the system to reach a state of minimum energy.

On the other hand, if energy absorbed by an activator in a crystal (a passive host) is transferred to a second activator of a different kind with the result that luminescence occurs in the second activator, the process is called *sensitized luminescence*. The activator that is responsible for the absorption of energy is called the *sensitizer*, and the activator that luminesces is the *emission center*. For this situation, the next stages occur: the absorption $g^s \rightarrow e^s$ transition is due to the sensitizer, an *energy transfer* process occurs from the sensitizer S to the center A in its higher-lying "excited" level. The level e^A populated by the energy transfer decays non-radiatively to the slightly lower (nr) , and finally the radiative emission, $(nr) \rightarrow g^A$, occurs.

Sometimes, the host lattice can function as the absorber in a luminescent system, that is, as an active matrix, in which case we refer to "*lattice-sensitized*" luminescence.

1.2. Configurational coordinate diagram (CCD)

For electronic transitions within a solid, it is very common to find bands rather than isolated absorption and emission lines. The configurational coordinate model is a model to explain the *width* of bands in solids, which should correspond to discrete levels such as is depicted next.

Figure 3 shows the configurational coordinate diagram (CCD) for a *single* metal ion (a luminescent center). The ordinate is the energy E of the activator-ligand system, whereas R (the configurational coordinate) is an interaction coordinate in the drawing and represents interatomic distance in a general way that defines the configuration of the ligands.

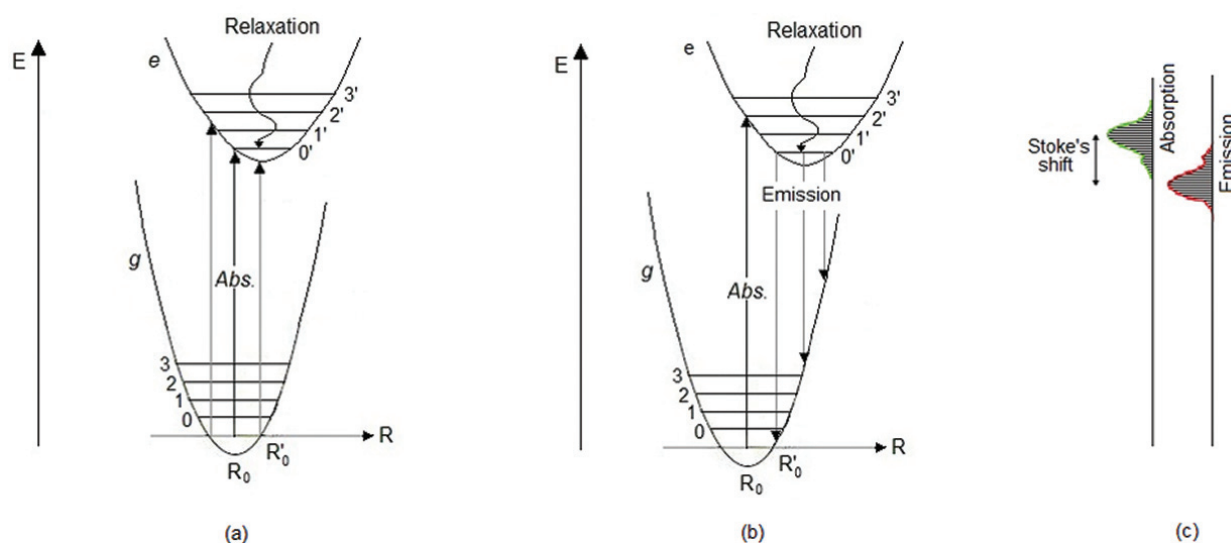


Figure 3. Configurational coordinate diagram showing (a) three vertical rows (absorption transitions) and (b) three vertical rows (emission transitions). (c) Stokes' shift between absorption and emission bands.

As a first approximation, for small displacements the center ion behaves as a harmonic oscillator. Their two electronic states are represented as parabolas. The equilibrium distance between the center ion and the ligand will be represented by a quantity R_0 for the g state, and to the first excited state (e) will be R_0' . The vibrational levels are shown by horizontal lines for both states (denoted by 0, 1, 2, 3 and 0', 1', 2', 3' the levels of g and e states, respectively). The absorption and non-radiative relaxation processes are indicated in **Figure 3(a)**. The vertical arrows represent the absorption of a photon (or energy from some other source: electric field, X-rays, neutrons, etc.) which excite a *single* center from the g state to the e state, and is usually referred as an optical absorption transition. Emission takes place as the electronic transition of the center from the lowest vibrational levels of the excited state to the ground state, **Figure 3(b)**.

However, the absorption, relaxation, and emission processes cover the dynamic behavior of all centers (metal ions) present in the solid, which is considered as a collective process. As the vibrations of the host lattice are random, they will affect the position of each center, so they will make different radiative transitions, depending on the value that the coordinate R takes.

If the luminescent material is cooled to 0°K, will only present electronic transitions between vibrational level lower of the ground state and the lowest vibrational level of the excited state, but at higher temperatures the vibrational coupling originates that electronic transitions made by all centers forming *bands* of excitation and emission into the solid in a continuous range of values of the energy [2]. The energy difference between the maximum of the absorption band and that of the emission band is called *Stokes' shift*; see **Figure 3(c)**.

This scheme of CCD assumes that there is an offset between the parabolas of the g and e states. *What does this mean?* In the next section, we focus the study on rare earth (RE) ions. Lastly on this section, the CCD will resume in the case of a crystal doped with a specific type of rare earth ions to show how the formation of bands in the crystal is due to this type of activators.

1.3. Luminescent properties of rare earth ions into a crystalline material

1.3.1. Chemistry of the rare earths

The rare earths (RE) elements are La, Ce, Pr, Nd, Pm, Sm, Eu, Gd, Tb, Dy, Ho, Er, Tm, Yb, and Lu, and can possess up to 14 identical electrons involving the *4f-shell*. All the REs exhibit the +3 valence state. The +4 and +2 valence states are stable mainly for RE ions with completely empty, half-full, or completely filled f shells, that is, $[\text{Xe}]4f^0$, $[\text{Xe}]4f^7$, and $[\text{Xe}]4f^{14}$ electron configurations. Examples are as follows: cerium has a stable 4+ valence state with a $4f^0$ electron configuration, and Eu^{2+} is the most stable divalent ion and has a $4f^7$ electron configuration (see **Table 1**). The RE^{3+} ions have the maximum possible numbers of unpaired f electrons (up to 7 for Gd^{3+}) and exhibit complicated magnetic behavior due, in general, that the electrons of the unfilled shells provide a net magnetic moment that may be oriented by the use of an *external magnetic field* B [3, 4].

1.3.2. Term symbols

For many-electron systems such as the transition metal, rare earth and actinide ions are considered, is convenient to represent the electron states with *term symbols* [5]. A *term symbol* has the general form $^{2S+1}L_J$, where $2S+1$ is the multiplicity of the term, S is the quantum

Z Element	Neutral atom configuration	(RE) ³⁺ configuration	Term (RE) ³⁺	(RE) ²⁺ configuration	Term (RE) ²⁺
57 La	4f ⁰ 6s ² 5d	4f ⁰	² F _{5/2}		
58 Ce	4f ¹ 6s ² 5d	4f ¹	² F _{5/2}		
59 Pr	4f ³ 6s ²	4f ²	³ H ₄	4f ³	⁴ I _{9/2}
60 Nd	4f ⁴ 6s ²	4f ³	⁴ I _{9/2}		
61 Pm	4f ⁵ 6s ²	4f ⁴	⁵ I ₄		
62 Sm	4f ⁶ 6s ²	4f ⁵	⁶ H _{5/2}	4f ⁶	⁷ F ₀
63 Eu ³⁺	4f ⁷ 6s ²	4f ⁶	⁷ F ₀	4f ⁷	⁸ S _{7/2}
64 Gd	4f ⁸ 6s ² 5d	4f ⁷	⁸ S _{7/2}		
65 Tb ³⁺	4f ⁹ 6s ²	4f ⁸	⁷ F ₆		
66 Dy	4f ¹⁰ 6s ²	4f ⁹	⁶ H _{15/2}	4f ¹⁰	⁵ I ₈
67 Ho	4f ¹¹ 6s ²	4f ¹⁰	⁵ I ₈	4f ¹¹	⁴ I _{15/2}
68 Er	4f ¹² 6s ²	4f ¹¹	⁴ I _{15/2}	4f ¹²	³ H ₆
69 Tm	4f ¹³ 6s ²	4f ¹²	³ H ₆	4f ¹³	² F _{7/2}
70 Yb	4f ¹⁴ 6s ²	4f ¹		4f ¹⁴	¹ S ₀
71 Lu	4f ¹⁴ 6s ² 5d	4f ¹³	² F _{7/2}	4f ¹⁴ 6s ¹	² S _{1/2}

Table 1. Electron configurations of RE ions in the ground state.

number of the total spin angular momentum, L represents the quantum number of the total orbital angular moment and is denoted by capital letters as follows:

- L : 0 1 2 3 4 5 6,...
- capital letter: $S P D F G H I$...

(It is an extension of the notation for a one-electron atom or ion: $s = 0$, $p = 1$, $d = 2$, etc.). J is the quantum number of the total angular momentum with allowed values being $|L-S|$, $L-S+1$, ..., $L+S-1$, $L+S$ [6].

The term symbols can be obtained using *Hund's rule*, which are of great help in evaluating the ground state of atomic or ionic systems [7]. They are stated as follows:

1. Terms allowed by the Pauli principle are ordered according to the quantum number S . The term of lowest energy level will be one of maximum value of S (highest multiplicity).
2. For two or more terms with the same maximum multiplicity that with greatest value of L will be the lowest energy level.
3. For configurations consisting of electrons in a *less than half-filled shell*, the ground multiplet (a term symbol) has the minimum J value, whereas for electron configurations with *more than half-filled shell* the multiplet has the maximum J value. That is, the lowest value of J is $|L-S|$ and its maximum value is $L + S$.

The term symbols are exemplified next. The Ce³⁺ ion (4f¹) contains a single electron into 4f-shell. Therefore, the quantum numbers: $S = 1/2 = s$ for the spin of an electron, $L = 3 = l$ (for one f

electron) and the values $J = j = l - s (=5/2)$, $l + s (=7/2)$. Thus, the term symbols to Ce^{3+} are ${}^2F_{5/2}$ and ${}^2F_{7/2}$, and they have the same multiplicity: 2. In agreement with third Hund's rule, ${}^2F_{5/2}$ term corresponds to the lowest energy level of the ground state.

Other case is to Eu^{2+} ion ($4f^7$), it has seven f electrons, first half-filled $4f$ -shell, and the lowest value for total orbital angular momentum is $L = 0$ and the highest value for total spin angular momentum is $S = 7/2$ and hence $J = |L \pm S| = 7/2$. Thus, the maximum multiplicity is 8, and ${}^8S_{7/2}$ is a single-term symbol corresponding to the ground state.

A third example: Yb^{3+} has the configuration consisting of 13 electrons. Using the *principle of equivalence of electrons and holes* [7], we obtain the term symbols ${}^2F_{5/2}$ and ${}^2F_{7/2}$. However, as the electrons are occupying more than half-filled $4f$ -shell, now, the lowest energy level will be ${}^2F_{7/2}$ (see the ground multiplet for Ce^{3+} , Eu^{2+} , and Yb^{3+} ions in **Table 1**).

A point to keep in mind: *Hund's rule is not to be applied to excited states*. Appendix 1, particularly, describes the terms that correspond to the electron configuration $4f^n$, being $n = 1, 2, 3, 4, \dots, 14$ for the rare earths.

The former two Hund's rule show their evidence: *the same largest $(2S + 1)$ occurs in several terms*. An example is Pr^{3+} ($4f^2$ electron configuration). Their terms are 1S , 1D , 1G , 1I , 3P , 3F , 3H (see Appendix 1). For this case, the largest multiplicity is 3, but the greatest value of L is 5(= H). Thus, the term multiplet is ${}^3H_{j=4,5,6}$.

1.3.3. Individual rare earth ions

To understand the energy levels of RE ions in a crystal, it is necessary to determine them in detail in the free atom. Since the lines originating are *intra- $4f^n$ configuration transitions* only, the energy levels of the f -shell have to be obtained [1, 8].

The Hamiltonian of a many-electron ion (assuming the nucleus fixed) in a magnetic field B is given by [4, 6]

$$H = \sum_i \frac{p_i^2}{2m} - \sum_i \frac{Ze^2}{r_i} + \frac{1}{2} \sum_{i>j} \frac{e^2}{r_{ij}} + \lambda \mathbf{L} \cdot \mathbf{S} \quad (1)$$

In Eq. (1), the first term represents the kinetic energy of the electrons, with $i = 1, 2, \dots, n$ electrons into d -shell, f -shell, and so on. The second is their Coulomb energy in the field of the nucleus. The third represents the energy associated with the mutual Coulomb repulsion between the electrons (electrostatic interactions), where the factor $1/2$ is justified by the Pauli principle [6]. The fourth is the spin-orbit interaction due to all the electrons, where λ is known as the *spin-orbit parameter*, and the \mathbf{L} and \mathbf{S} vectors are the total orbital and spin angular momenta, respectively. This interaction is denoted as H_{so} .

For the magnetic ions of much interest such as rare earth and transition metal ions, the next assumption is appropriate: the electrostatic interactions are certainly larger than the magnetic interactions [4]. Particularly, in rare earth ions, spin-orbit interaction is much smaller than electrostatic interaction, and, however, this must be taken into account due to coupling between \mathbf{L} and \mathbf{S} .

The energy levels of the free ion, such as an RE or a transition metal ion, in the absence of spin-orbit interaction, are characterized by different terms ^{2S+1}L . *What does this mean?*

Example. Consider us again the Ce^{3+} ion. When the spin-orbit interaction is taken into account over the $4f^1$ level, it splits in other two levels, $^2F_{5/2}$ and $^2F_{7/2}$.

The total angular momentum vector is $\mathbf{J} = \mathbf{L} + \mathbf{S}$. The eigenvalues of the $\mathbf{J} \cdot \mathbf{J}$ operator are $J(J+1)$ and in similar way $\mathbf{L} \cdot \mathbf{L}$ have eigenvalues $L(L+1)$, and $\mathbf{S} \cdot \mathbf{S}$ to the $\mathbf{S} \cdot \mathbf{S}$ operator [6]. Using the relation

$$2\mathbf{L} \cdot \mathbf{S} = (\mathbf{L} + \mathbf{S}) \cdot (\mathbf{L} + \mathbf{S}) - \mathbf{L} \cdot \mathbf{L} - \mathbf{S} \cdot \mathbf{S} = J(J+1) - L(L+1) - S(S+1) \quad (2)$$

It can be shown that, for example, with λ positive, for the single electron in $4f$ -shell of Ce^{3+} , the energy level to $J = 7/2$ is higher than that to $J = 5/2$, by $7\lambda/2$ due to the perturbation $\lambda \mathbf{L} \cdot \mathbf{S}$.

1.3.4. Crystal field theory

Crystal field theory is based on the hypothesis that a magnetic ion (an RE, a transition metal, or an actinide ion) in a crystal site feels the influence of its neighbors, the ligand ions, as an electric field which has the symmetry of the site. RE ions in crystals present spectra which are *sharp f-f transition* similar to free atoms [1, 3]. This is a consequence of the shielding of the $4f$ -shell from the surroundings by the filled $5s$ and $5p$ shells.

When RE ions are embedded in a host, crystal field $\mathbf{H}_{\text{cryst}}$ effects are small (typically 100 cm^{-1}) because f electrons are deeper in the ion [1, 8]. Hence, the spin-orbit interactions would be stronger due to the electrons that are nearer to nucleus: $\mathbf{H}_{\text{cryst}} < \mathbf{H}_{\text{so}}$.

The effects of crystal field strength and spin-orbit interaction are important, according to the order of magnitude [1, 3]. Thus, $\mathbf{H}_{\text{cryst}}$ is included in the Hamiltonian as follows:

$$H = \sum_i \frac{p_i^2}{2m} - \sum_i \frac{Ze^2}{r_i} + \frac{1}{2} \sum_{i>j} \frac{e^2}{r_{ij}} + \lambda \mathbf{L} \cdot \mathbf{S} + \mathbf{H}_{\text{cryst}} \quad (3)$$

For instance, consider the CaS:Eu luminescent compound. The CaS host lattice has the NaCl structure; therefore, each one of Eu^{2+} ion prefers to occupy the Ca^{2+} site, because the ionic radii of Eu^{2+} (1.12 \AA) is compatible with those of Ca^{2+} lattice site and it has an octahedral symmetry as shown in **Figure 4**. In this situation, the $^8S_{7/2}$ level (orbitally nondegenerate, because $L = 0$) of the ground state is very stable and cannot be *split* by the crystal field.

1.4. Absorption and emission spectra of RE ions in crystals

1.4.1. Intraconfigurational- $4f^n$ transitions: narrow absorption and emission lines

Figure 5 shows an energy-level diagram for some RE^{3+} ions. The effect of crystal field is very small, but produces a *splitting* on these energy levels to each one of RE^{3+} (Gd^{3+} is an exception; it has seven electrons in $4f$ -shell, and thus the $^8S_{7/2}$ level of the ground state is very stable). The electronic transitions within the $4f$ -shell are only weakly influenced by crystal fields and

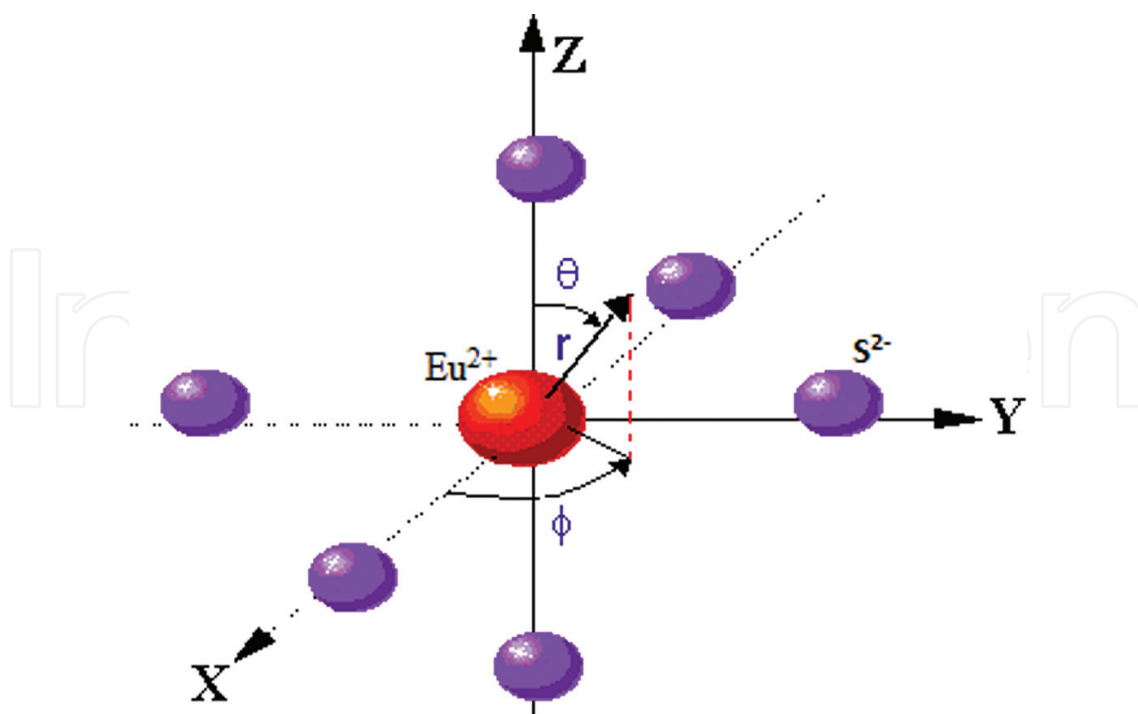


Figure 4. Eu^{2+} (central ion) substitute for Ca^{2+} lattice site has octahedral symmetry around six S^{2-} ligands.

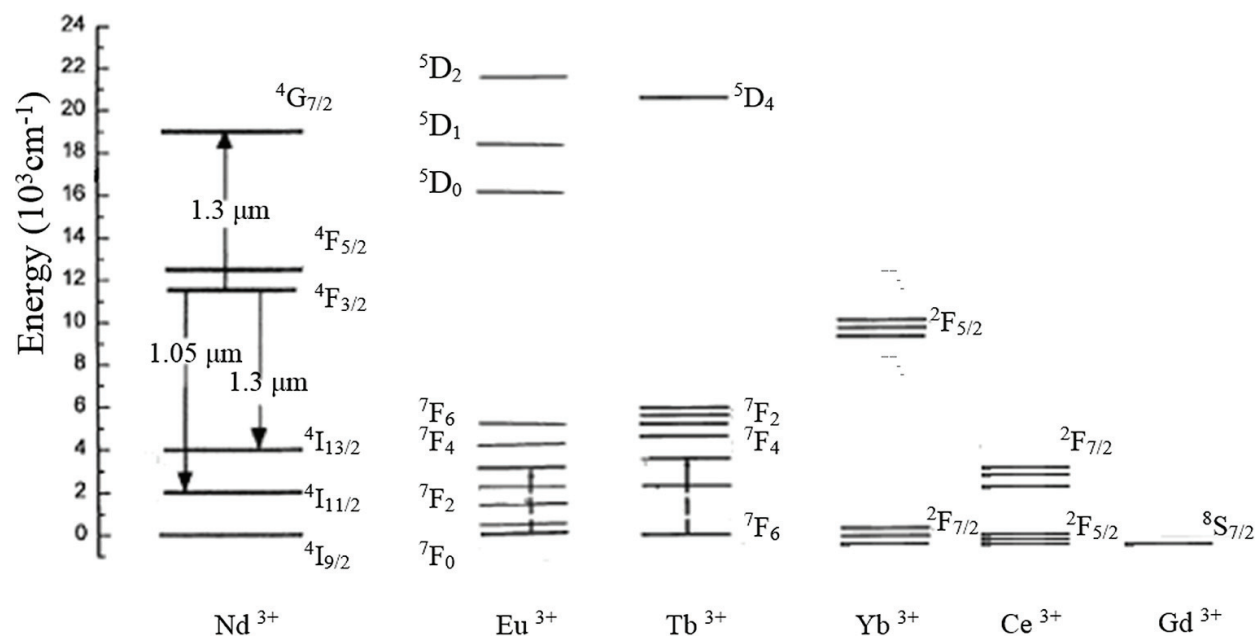


Figure 5. Energy-level diagram of rare earth ions: Nd^{3+} , Eu^{3+} , Tb^{3+} , Yb^{3+} , Ce^{3+} and Gd^{3+} .

covalency effects [1, 4]. Actually, $\Delta R = R(e) - R(g) \sim 0$, the change in configurational coordinate between ground and excited states is very small or zero, so that narrow absorption and emission lines will be observed, rather than broad bands as is shown on the left-hand side of Figure 6(a) [2].

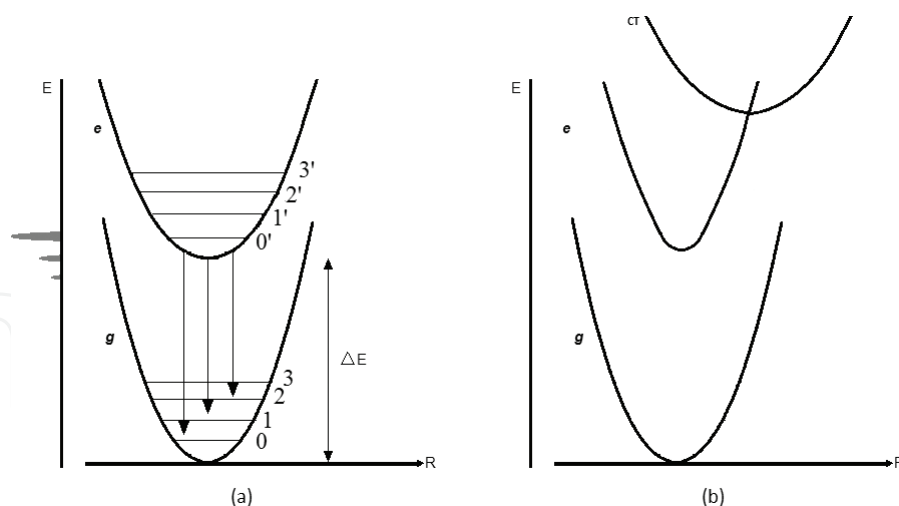


Figure 6. (a) In a CCD, these levels appear as parallel parabolas. On the left-hand side of **Figure 6(a)**, narrow lines appear due to *intra-4fⁿ configuration transitions*. (b) The charge-transfer state has a larger offset (highest parabola).

1.4.2. Interconfigurational transitions: absorption and emission bands

The allowed optical absorption transitions of the rare earth ions are *interconfigurational* and consist of two different types: $4f^n \rightarrow 4f^{n-1}5d$ transitions and charge-transfer transitions ($4f^n \rightarrow 4f^n +1L^{-1}$, where L denotes an anion such as Cl^- , S^{2-} , O^{2-} , etc.) [1, 2].

1.4.2.1. $4f^n \rightarrow 4f^{n-1}5d$ transitions

The $4f^n \rightarrow 4f^{n-1}5d$ transitions are strongest in rare earth that have a tendency to become divalent (from RE^{3+} to RE^{2+}), such as Eu^{2+} , Sm^{2+} , and Yb^{2+} , where broad and intense absorption bands are observed in the UV of electromagnetic spectrum.

Example 1: Eu^{2+} ions into a host lattice. Its interconfigurational transition $4f^7 \rightarrow 4f^65d$ corresponds to a *broad absorption band*, and it shows an $5d \rightarrow 4f$ emission band which can vary from UV-yellow range of the electromagnetic spectrum.

Example 2: Ce^{3+} ions into a crystal. Remember the next: spin-orbit coupling causes $^2F_{5/2}$ and $^2F_{7/2}$ levels of the ground-state configuration ($4f^1$) of Ce^{3+} ion. The crystalline field yields a splitting of the configuration ($5d^1$) in several levels. Thus, due to $4f \rightarrow 5d$ transitions, absorption bands appear in the UV region of electromagnetic spectrum because Ce^{3+} tends to become tetravalent. Hence, the luminescent spectrum contains two *sharp emission bands* due to next transition: from the lowest $5d$ crystal field level to the ground state ($4f^1$).

1.4.2.2. Charge-transfer transitions

Figures 3 and **6(a)** have been referred to two different schemes on configurational coordinate diagram: the former for two non-parallel parabolas and the second one to parallel parabolas. Now, we consider a suitable concentration *centers* inside host lattice, schematized through three parabolas as shown in **Figure 6(b)**. What does the highest parabola mean?

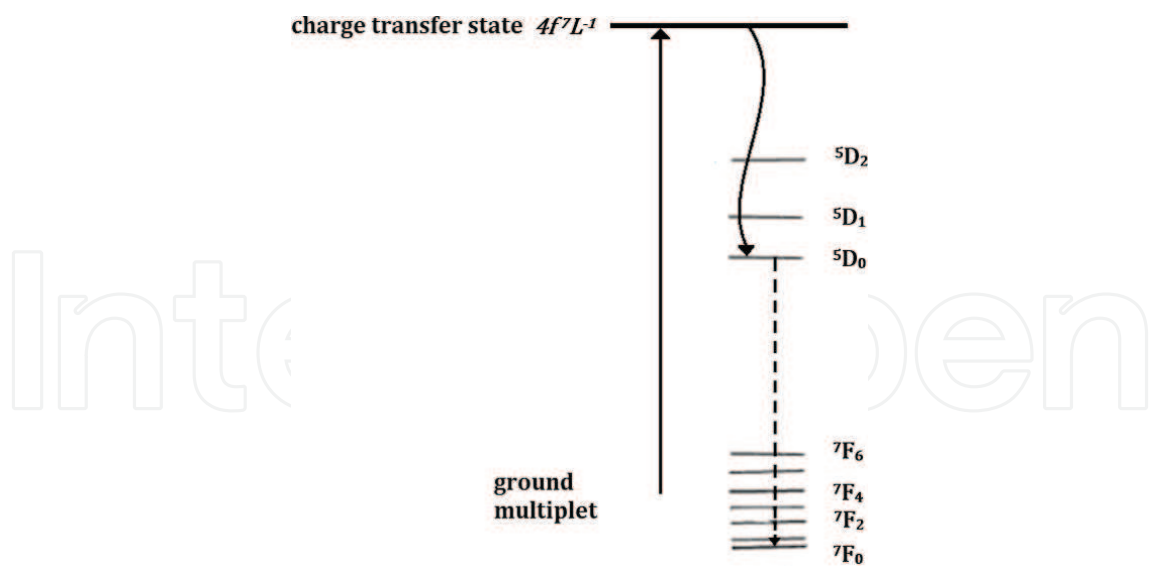


Figure 7. The role of charge-transfer state. It populates, at least partly, the ground-state levels ${}^7F_{J=0,1,2,3,4,5,6}$ of the electron configuration of the Eu^{3+} .

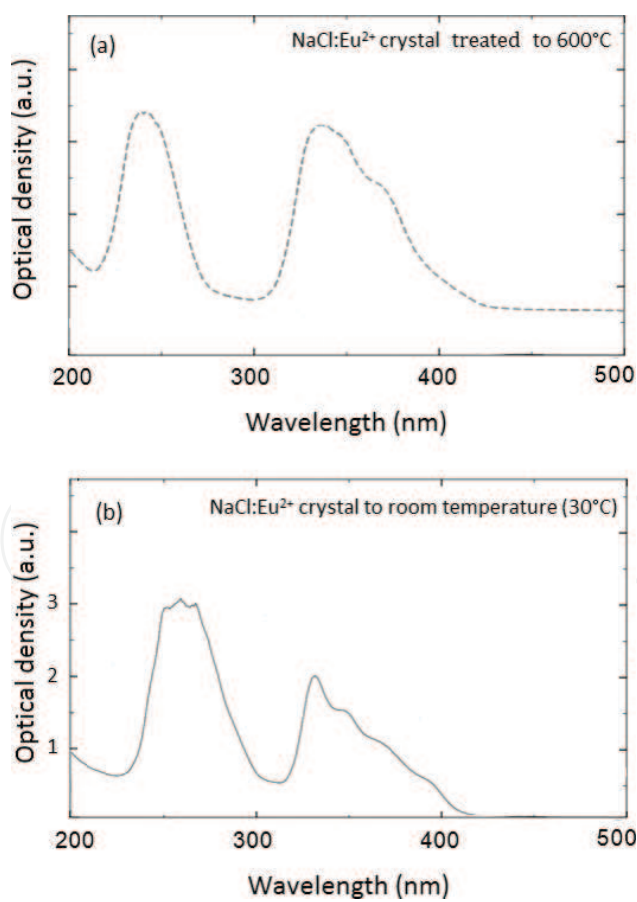


Figure 8. Both absorption spectra consist of two bands: (a) $\text{NaCl}:\text{Eu}^{2+}$ crystal to 600°C and (b) $\text{NaCl}:\text{Eu}^{2+}$ without treatment thermal.

Intraconfigurational- $4f^n$ transitions (the two parallel parabolas) yield very weak emission lines. In this scheme, the non-parallel parabola means a *charge-transfer state*, which originates from a different configuration and is connected to the $4f^n$ configuration by an allowed transition as follows. *Excitation* occurs now from the ground state to the charge-transfer state (hence the yield of the *absorption band* is a charge-transfer transition in the $RE^{3+}-L^-$ bond, L being an anion such as Cl^- , S^{2-} , O^{2-} , etc.). From here, the system relaxes to the relaxed excited state of the second parabola (the *non-radiative transition* between the two upper parabolas is possible). *Emission* occurs from the second parabola (*line emission*) to the lower parabola.

For example, consider an Eu^{3+} ions-doped host lattice. Levels of the ground state ($4f^6$) of Eu^{3+} , according to Appendix 1, are 7F , 5D , and so on. Luminescent processes are $^7F_J \rightarrow$ charge-transfer state *excitation*, charge-transfer state \rightarrow 5D_0 *relaxation*, and $^5D_0 \rightarrow$ 7F_0 *emission*. **Figure 7** shows some energy level of Eu^{3+} in a certain semiconductor crystal.

Luminescence process can occur, mainly, because the host contains an *appropriate concentration of ions* which luminesce. Also, bands involved in an absorption spectrum maintains a *dependence with the temperature* [7]. Consider the next example.

*A previous example to the results, which is presented in Section 2.1, is referred to an NaCl crystal doped with Eu^{2+} . This crystal has dimensions of $8 \times 8 \times 1$ mm³, and grows by the Czochraski method. The concentration of Eu^{2+} aggregated to the powder of NaCl was of 0.1 wt%. This sample was heated in the seven next stages: 100, 240, 340, 390, 440, 540, and 600°C. All absorption spectra consist of two bands in the range of 200–440 nm, but in **Figure 8(a)** only the spectrum referred to 600°C is shown. With respect to the spectrum of continuous curve shown in **Figure 8(b)**, the high-energy band lost its structure in relation to the relative maxima observed in the continuous curve and the low-energy band does not considerably change its structure with such treatments [9, 10]. Remark: the high-energy band has shown a dependence with the treatment temperature.*

1.5. Types of luminescence spectra and its relationship with photoacoustic technique

In this section, we review some techniques related with the luminescent spectra for measuring PL decay lifetimes, time-resolved PL, and photoacoustic (PA) spectra.

1.5.1. Technique of optical absorption

1.5.1.1. Theoretical model

For a homogeneous material, the relative fraction of the light intensity absorbed in traversing a thickness dx depends on absorption coefficient α (a constant characteristic of the material) as follows:

$$\frac{dI}{I} = -\alpha dx \quad (4)$$

Thus, if the incident photons intensity at the sample surface is $I_0 = I(x = 0)$ and I is the transmitted intensity, we obtain Eq. (6):

$$I(x) = I_0 e^{-\alpha x} \quad (5)$$

Transmittance is defined as $(\frac{I}{I_0})100\%$, but also the optical density (OD) is often used:

$$\text{OD} = \ln\left(\frac{I_0}{I}\right)/2.303 \quad (6)$$

where the reflection at the sample surface is neglected for simplicity (so, e.g., 1% transmittance corresponds to an OD = 2). Of Eqs. (6) and (7), the absorption coefficient can be expressed as

$$\alpha = \left(\ln\left(\frac{I_0}{I}\right)\right)/x, \quad (7)$$

with α in cm^{-1} . For example, if the thickness of an amorphous film is 1 μm and $\alpha = 100 \text{ cm}^{-1}$, thus, the transmittance is 99%.

1.5.1.2. Experimental equipment

The absorption spectrophotometer equipment often measures the quantity OD.

1.5.2. Technique of photoluminescence

Consider again a two-level system: the ground state (g) to refer to a level in the ground state, and (e) for another level but in the excited state. Consider N_i to be the number of centers that exist in the host lattice. At the time of excitation of the sample with light coming from a power source, a fraction f of the total centers will be taken from g to e state, and will occur after a *stimulated emission* from e to the g state. This process will continue until the condition of an equilibrium is established:

$$fN_i = (C_g + C_e) \quad (8)$$

That is, the total number of centers that succeeded to pass through level g to level e . C_e is a number of centers in the state e and a number C_g in the ground state that made it through the level g [10].

The energy gap between the levels e and g is the energy of emission of centers and is given by the equation

$$E_{\text{photon}} = hc/\lambda \quad (9)$$

λ being the wavelength of the emitted light and hc is a constant depending on the system of units used (if E_{photon} is expressed in cm^{-1} and λ is in nm then the constant hc has the value 10^7 , and when E_{photon} is measured in eV, the constant hc has the value 1239.8 eV-nm].

On the other hand, the intensity of emission I due to n photons emitted every interval of time t is

$$I = \frac{n}{t} \quad (10)$$

In these circumstances to say, the intensity of emission I reaches the value of *steady state* [2, 10].

The process of excitation emission to measure the photoluminescence spectra is schematized in **Figure 9**.

1.5.3. Techniques of time-resolved photoluminescence

1.5.3.1. Theoretical aspect

For the two-level system, e and g , the population of the excited state decreases according to [2, 10]

$$\frac{dn}{dt} = -P_{eg}n \quad (11)$$

In Eq. (5), the value of n gives the number of luminescent centers in the excited state after an excitation pulse, t is the time, and P_{eg} the probability for *spontaneous* (or radiative) *emission* from the excited to the ground state. Integration yields

$$n(t) = n(0)e^{-\frac{t}{\tau}} \quad (12)$$

$\tau = 1/P_{eg}$ being the *radiative decay time*. The emission intensity is the rate of decay of the population of the excited state, that is,

$$I = -\frac{dn}{dt} \quad (13)$$

$$I = \frac{n(0)}{\tau} e^{-\frac{t}{\tau}} \quad (14)$$

1.5.3.2. Experimental

The time-resolved PL spectroscopy is very productive for obtaining the recombination rates (or lifetimes) of various transitions. Thus, determining the dynamical processes including

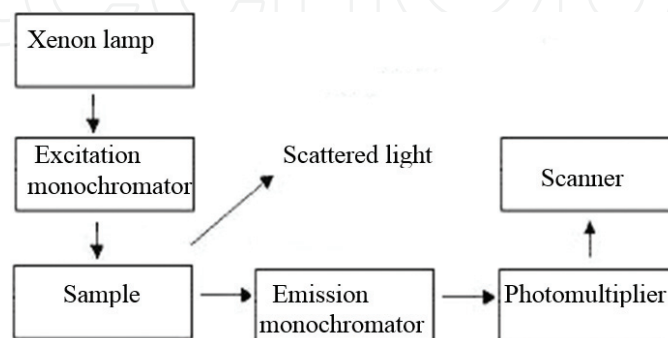


Figure 9. Schematic diagram of a spectrofluorimeter brand SPEX Fluorolog to obtain the excitation-emission spectra of the phosphor materials.

emission line energies and the associated recombination rates as well as quantum efficiencies is one of the basic purposes of time-resolved PL studies [11].

Time-resolved PL spectroscopy (or *pulsed laser-excited time-resolved luminescence*) is a relatively new technique usually paired with pulse laser excitation. If the laser pulse is brief enough (typically a few nanoseconds), the excitation is considerably shorter than most excited state lifetimes, offering the possibility of separating emission from different electronic states. In practice, this technique is applied by the synchronous use of laser pulses and gated detectors. One-timed signal will activate the laser, while the next, after a predetermined wait, will turn on the detector. Another signal will turn off the detector after a set dwell period. In this way, over many thousands of pulses, a complete emission spectrum can be acquired from electronic states with certain lifetimes. This is a particular value when trying to sort out the emission of activators whose emission spectra heavily overlap but differ in lifetime. **Figure 10** shows an arrangement for obtaining the time-resolved PL spectra.

1.5.4. Photoacoustic spectroscopy

1.5.4.1. General description

The photoacoustic spectroscopy (PAS) of solid materials was revived around the year 1970, and is widely used in the research of amorphous films to investigate the phenomena physical and chemical in a number of fields including biology and medicine. More frequent use photoacoustic detection mode includes a microphone of gas cell, and is unique because it makes a direct monitoring of non-radiative relaxation and hence channel that complements the spectroscopic techniques of optical absorption and photoluminescence. This complementarity is because the PA spectrum is a spectrum of excitation which is related to the amount of heat generated by many non-radiative processes [12, 13].

1.5.4.2. Experimental

This technique is used to obtain optical absorption spectra more defined near the *edge of absorption*, from which E_g , the bandwidth of optical energy [12], can be calculated.

The PA spectrometer consists of a stabilized 1000-W Xe lamp and a (1/8)-m-grating monochromator (Oriel, Model 77250). The monochromatic output beam was intensity modulated at 17

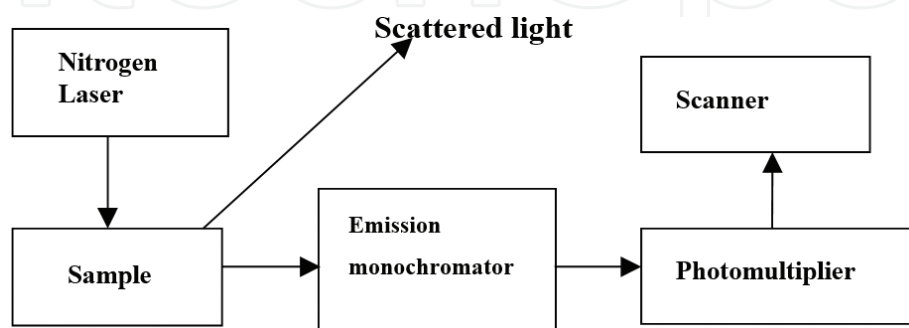


Figure 10. Arrangement for measuring PL decay and PL emission intensity at different delay times.

Hz with a mechanical chopper. The PA signal is recorded by an electret microphone and a lock-in amplifier. More details of this technique will be reviewed in Section 2.2.3.

1.6. Luminescent glasses

The preceding sections have dealt exclusively on solids in their crystalline form. However, also many glassy solids are of practical use today rather than crystalline.

When a liquid solidifies without crystallizing, it is currently said to form a *glass*, that is, to *vitrify*, or to pass to a *vitreous state*. This definition was initially reserved for inorganic solids, but such definition is too restrictive, due to that a large number of organic liquids also form glasses [14, 15].

Most of the inorganic glasses encountered in the laboratory or in daily life are composed of mixed oxides of several elements. The oxides are usually described as the anion or polyanion of a nonmetallic element of high electronegativity (silica, borate, silicate, phosphate, germanate, and tellurite glasses). Examples of oxide glasses are SiO_2 , B_2O_3 , P_2O_5 , $\text{SiO}_2\text{-Na}_2\text{O}$, $\text{TeO}_2\text{-V}_2\text{O}_5$, $\text{B}_2\text{O}_3\text{-Al}_2\text{O}_3\text{-CaO}$, $\text{TeO}_2\text{-GeO}_2\text{-ZnO}$, and $\text{PbO-P}_2\text{O}_5\text{-TeO}_2$ [14, 15].

Like crystals, glasses consist of an extended three-dimensional *network* but the diffuse character of the X-ray diffraction (XRD) spectra shows that the network is not symmetric and periodic as in crystals (i.e., there is no long-range order).

The glass network may be compared to a unique molecule or a system with a giant unit cell. Its structure can be analyzed in terms of *coordination polyhedra* of cations surrounded by a variable number of anions. In crystalline solids, polyhedra can have common corners, edges, or faces. For example, in NaCl crystals, each *octahedron* consists of six Cl^- ions surrounding Na^+ cation.

Zachariasen sought the manner in which the polyhedra could be joined to build a disordered network related to that of a crystal [15]. For instance, SiO_2 in their different *crystalline forms* (quartz, cristobalite, tridymite, etc.), its network is built with SiO_4 *tetrahedra* (four oxygen ligands to a single *Si* form a single tetrahedron) joined at their corners. The same is true for *vitreous* SiO_2 but due to its non-periodicity, the mutual orientation of the consecutive tetrahedra is variable.

According to Zachariasen, the term *network former* has been adopted for an oxide which belongs to vitreous network, and *network modifier* for an oxide which does not participate directly in the network [15]. Certain oxides can function as glass formers or as modifiers depending upon the glass compositions involved. They are called *intermediate oxides*. **Figure 11** classifies some oxide compounds as glass formers, modifiers, and intermediates [14].

In particular, oxide compounds such as SiO_2 , B_2O_3 , P_2O_5 , and GeO_2 alone have the ability to form glass, and when mixed with other oxides such as those of alkaline metals, alkaline earth metals, and transition metal form glasses [15]. These are the *classic or conventional glasses* that are referred in the literature as *silicate*, *borate*, *phosphate*, and *germinate* glasses, respectively. On the other hand, oxides TeO_2 , V_2O_3 , SeO_2 , MoO_3 , and Bi_2O_3 are known as *conditional network formers* not able to vitrify themselves when a *conventional melt-quenching method* of

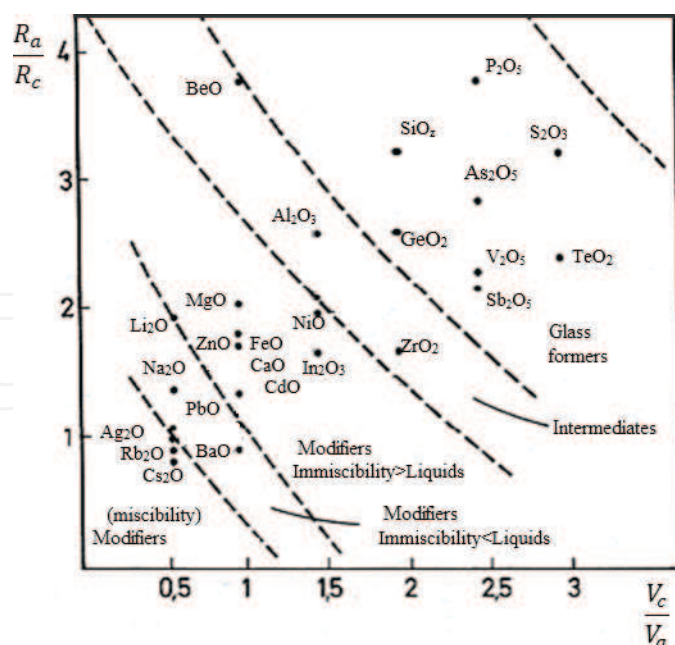


Figure 11. Classification of some oxide compounds in accordance with the role played in the glass formation.

vitrification is used, but when mixed with other oxides they are so-called *non-conventional* glasses [16].

Consider now TeO_2 , a conditional network former. The structure of TeO_2 *crystalline* consists of trigonal di-pyramids (tdp) TeO_4 . **Figure 12** shows a tdp: the equatorial plane is occupied by the lone pair of electrons (*5s-electrons*) of the tellurium atom and two atoms of oxygen $\text{O}_{\text{eq}}\text{-Te-O}_{\text{eq}}$ and in the axial positions are occupied by two atoms of oxygen $\text{O}_{\text{ax}}\text{-Te-O}_{\text{ax}}$ [17]. X-ray and neutron diffraction structural studies have shown that the atomic arrangement in glassy TeO_2 may be well described as a three-dimensional network of TeO_4 tdp [18, 19].

Actually, a *tellurite glass* is constituted by TeO_2 in high percentage and other network nonformer oxides as second component, third component, and so on. The structural units of *tellurite glasses* are assumed to be TeO_4 and trigonal pyramids TeO_3 , the latter with three bond Te-O shorter distances concerning the TeO_4 , where it has been observed that a change of TeO_4 in TeO_3 happens when the *modifier oxide* (a second component) content increases at the expense of that high content TeO_2 decreases [20]. **Figure 13** shows that the polyhedra could be joined to build a disordered network in tellurite glasses. The relative abundance of these units depends on the composition [21]. Section 2.2 presents the photoluminescence and photoacoustic spectra (PAS) measured of a type of tellurite glasses.

Some glass-forming oxides, for examples, TeO_2 , B_2O_3 , S_2O_3 , in themselves *do not luminesce*, but the presence of suitable activators leads to numerous interesting phenomena. Contrary to the case of crystalline solids, the lack of periodicity in atomic arrangements in glasses leads to a *broadening* of the luminescence spectra. Glasses are an intriguing material with which to study luminescence phenomena; however, their power of dissolving most additives makes systematic studies of the effect of composition and, hence, of structure on luminescence possible [14, 22].

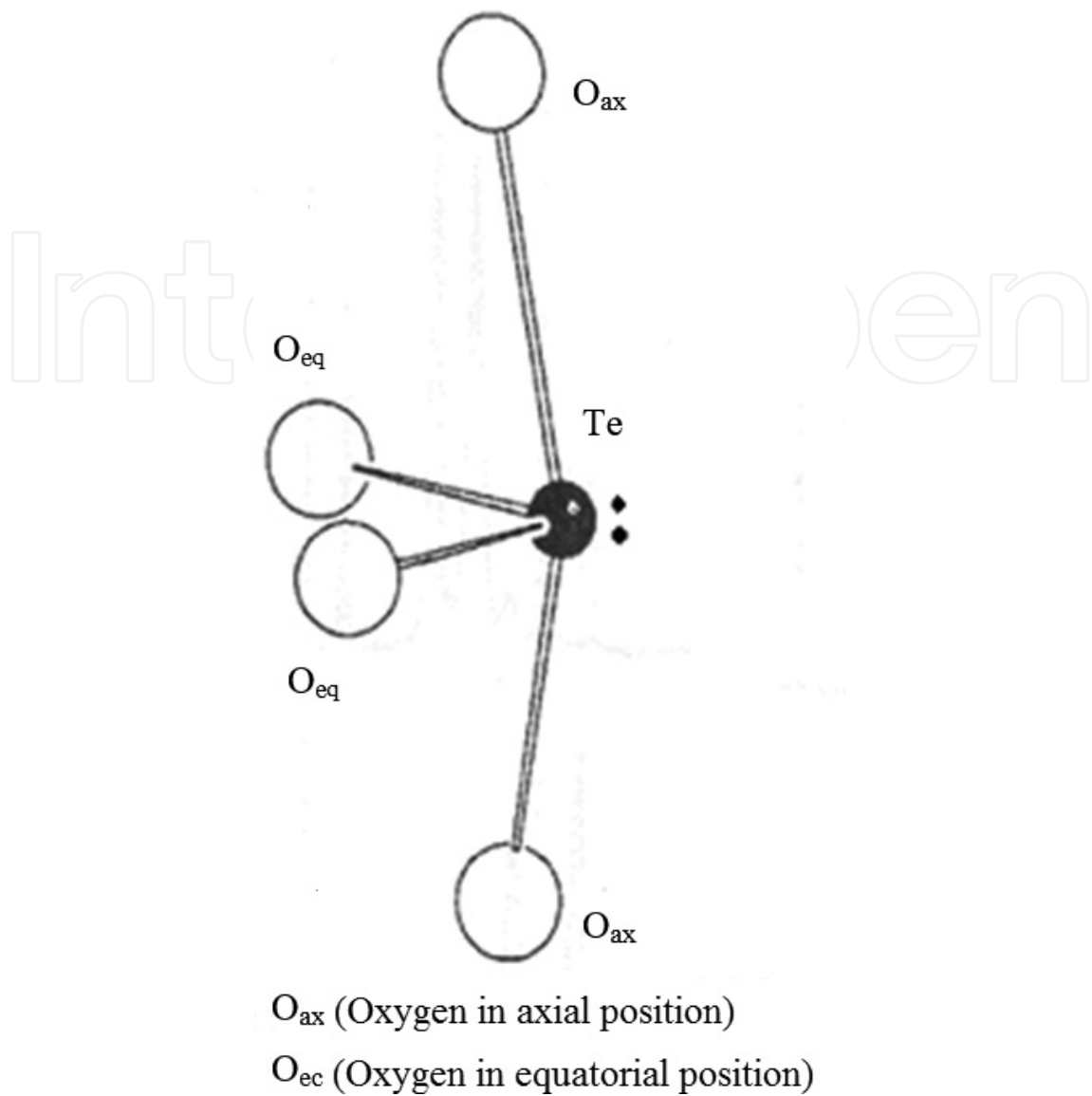


Figure 12. Structural model for TeO_4 units in TeO_2 crystalline: the Te presents coordination four with the first neighbors (the four oxygen), which are occupying four of the vertices of the tdp. These units form a three-dimensional-ordered network, which is not shown here.

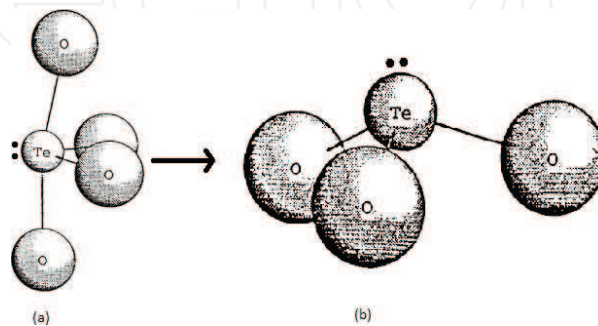


Figure 13. In the structure of glasses with containing high amount of TeO_2 , the building units of these materials are (a) TeO_4 and (b) TeO_3 groups. TeO_4 represents the partial transformation of TeO_3 units due to the incorporation of a *modifier* of the network in a tellurite glass.

Luminescent centers in a host glassy consist of (a) “energetically isolated” activators, such as metal atoms, which may be considered to exist as a metal vapor in the glass, (b) molecules or groups that possess such a highly covalent nature as to be considered molecular groups, and (c) ions that participate directly in the glass structure and are, thus, more greatly affected by the host glass composition. In the latter case, the *luminescence of rare earth ions* is influenced by changes in glass structure less than that of other ions because of the shielding of the inner $4f$ electrons in which the transitions leading to emission occur. Rare earth ions can be easily incorporated into many glasses, so these materials represent in principle an interesting area of research. In a host glassy, the local environment of a rare earth ion is roughly the same as that in a crystal, giving rise to a spectrum consisting of distinct lines.

Luminescent glasses serve as a useful function in products such as lasers, dosimeters, scintillation counters, artificial teeth, and electroluminescent devices. Furthermore, luminescent glasses are useful in research for studying such problems as the constitution of glasses and the formation of a vitreous phase in a crystalline substance.

2. Experimental results

This section covers the results on the study in luminescent materials doped with a rare earth compound (with an appropriate concentration of RE ions). In order to start using some techniques of photoluminescence, a first result of my research presents the time-resolved photoluminescence spectra of an alkali halide crystal doped with Eu^{2+} ions; the next results on photoluminescence and photoacoustic were obtained for oxide glassy compounds containing a concentration of a one type of rare earth ions.

2.1. Results of time-resolved PL spectroscopy: NaCl:Eu^{2+} crystal

Consider the NaCl:Eu^{2+} luminescent compound as an example. EuCl_2 was added to the powder of NaCl . The Eu^{2+} ions enter the NaCl network and substitute some Na^+ ions during the crystal growth [9, 10]. The concentration of Eu ions into the NaCl powder was of 0.1 wt%.

In this section, the results of luminescent decay and spectral measures with temporal resolution (pulsed luminescence) are presented, in order to corroborate the fact that the Eu centers have a different interaction with the environment (Cl^- ligands and cation vacancies). To measure the decay of luminescence, the crystal was exposed to 500-ps and 337-nm laser pulses sent to the crystal with a frequency approximate of 10 pulses/s. By every pulse of excitation that makes a measure of intensity, this means that the intensity of the emitted light could vary according to the intensity of the pulse. For the analysis of the measures, the intensity of the excitation pulse has been considered constant. In this way, already every measure of intensity corresponding to a single pulse, intensity can be seen in relative and in this way we obtain the set of measures that represent the decay of the broadcast of the crystal at a fixed wavelength. Taking into account the luminescence results reported in the interval (380, 540) nm, the emission monochromator was set at corresponding wavelength of luminescence spectral region [9]. In **Figure 14**, a particular case of luminescent decay occurs on a semilogarithmic

plot. As a way of presenting, it is to be noted that the decay of the intensity is very approximately exponential, in agreement with Eq. (15). These measures correspond to a freshly annealed crystal of 600°C to room temperature and to 427-nm emission wavelength. The slope of the graph obtained by least squares adjustment turned out to be 1.10 μs , which coincides within the experimental error with that reported as in [23]. Measures of decay emissions taken between 400 and 500 nm showed times of life around 0.85 μs to the crystal without treatment thermal.

Using the technique of temporal resolution, the *emission spectra* in the region of 390–490 nm were obtained. Two typical examples are presented in **Figures 15** and **16**. Curves in **Figure 15** correspond to the newly annealed crystal and those in **Figure 16** to the crystal without heat treatment. Both curves in **Figures 15** and **16** were taken with 100- and 1300-ns delay times. We see a similar behavior in both cases. In the case of the newly annealed crystal, it dominates the

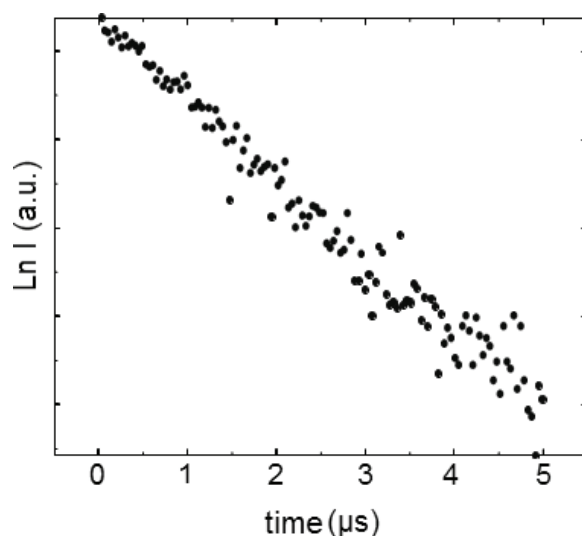


Figure 14. Temporal response of PL emission from a NaCl:Eu^{2+} freshly annealed crystal to 600°C (to a light emitted in 427 nm).

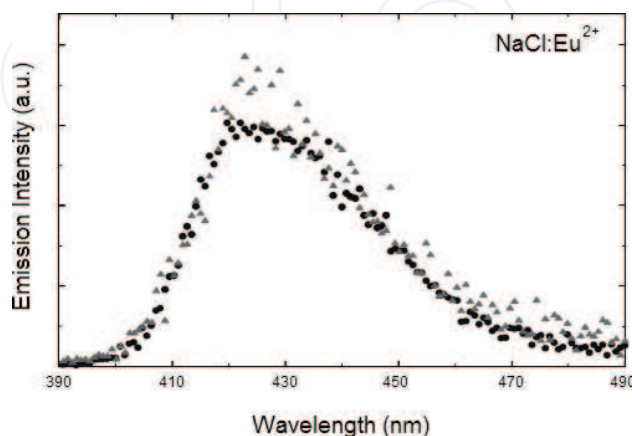


Figure 15. Emission spectra of a NaCl:Eu crystal freshly annealed crystal to 600°C with a temporal resolution of 100 (circles) and 1300 ns (triangles).

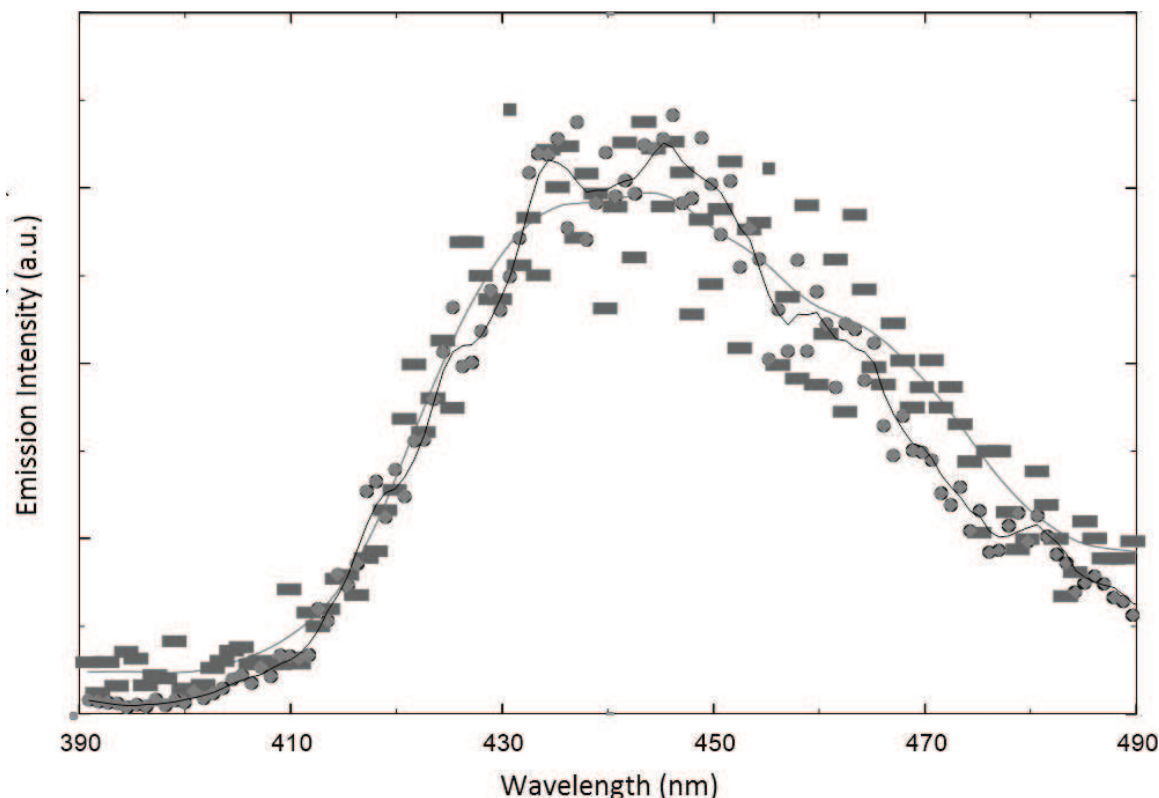


Figure 16. Emission spectra of a *NaCl:Eu* crystal without prior heat treatment, with a temporal resolution of 100 (circles) and 1300 ns (rectangles).

emission of free dipoles, while in the case of unheated crystal, it dominates the aggregate emissions [10].

2.2. Results of the photoacoustic and photoluminescence spectra of rare earth ions-doped cadmium-tellurite glasses

Research on tellurite glasses is currently being performed because several of its properties can be used in different types of modern devices [24–26]. These glasses show wide transmission in the 0.4–5.0- μm range, high linear and nonlinear refractive index, good corrosion resistance, thermal and chemical stability, and they are capable of incorporating large concentrations of rare earth ions into the matrix [27, 28]. Tellurite glasses represent a compromise between the desire for a low phonon energy host (800cm^{-1}) coupled with the need to retain mechanical strength and low-processing temperatures [29]. When tellurite glasses are doped with rare earths, high-intensity, narrow-peak emissions can be obtained. This last property makes these materials good candidates for laser applications [30].

RE^{3+} -doped zinc-tellurite glasses have been studied for $\text{RE} = \text{Nd}$ [31].

The following results are part of a wide research about the study of a ZnO-CdO-TeO_2 ternary system doped with rare earth ions. Four papers have been published early in the which the photoluminescence properties, structural studies, optical, and thermal analysis about this

Sample	V1	V2	V3
ZnO	9.52	9.52	9.52
CdO	9.52	19.04	28.58
TeO ₂	76.20	66.68	57.14
REc	4.76	4.76	4.76

REc (rare earth compound): Tb₄O₇, YbBr₃, NdCl₃, EuCl₃. Their concentrations are (2.5, 2.9) range mol%.

Table 2. Bath original compositions (wt%) of ZnO-CdO-TeO₂:REc glasses.

matrix containing ytterbium and terbium [32, 33], neodymium [34], and europium ions [35] are reported.

Particularly, *tellurite glasses in the glass-formation region* (near the corner rich in TeO₂ in a composition triangle), for the ZnO-CdO-TeO₂ system, have been studied [36].

2.2.1. Conventional melt-quenching method

Three batches of ZnO-CdO-TeO₂ system were prepared, as can be seen in **Table 2**, by mixing appropriate amounts of the oxides: TeO₂ 99.999% purity (Sigma Aldrich), CdO 99.999% purity (Sigma Aldrich, St. Louis, MO), ZnO 99.5% purity (Merck, Dakota, MN), and a rare earth (Yb, Tb, Nd, or Eu) compound 99.99% purity (Alfa Aesar, Ward Hill, MA). The glasses were fabricated by using a conventional melt-quenching method in a platinum crucible in the 1000–1200°C range.

Remark: V1, V2, and V3 glasses containing Tb³⁺ ions are referred as Tb118, Tb127, and Tb136, respectively; meanwhile, those doped with Yb³⁺ ions are Yb118, Yb127, and Yb136. However, V1, V2, and V3 denote the other two types, glasses containing Nd³⁺ or Eu³⁺. All the measurements were recorded at room temperature.

2.2.2. XRD results on ZnO-CdO-TeO₂:REc glasses

These results are summarized as follows:

- a. Yb118, Yb127, and Yb136 glasses display the pattern of an amorphous structure, and small particles of CdTeO₃ crystals are observed in the sample Yb118, see Refs. [32, 33].
- b. Tb118, Tb127, and Tb136 glasses also show a crystalline phase CdTeO₃, see Refs. [32, 33].
- c. Of the V1, V2, and V3 glasses containing Nd³⁺, all exhibit a vitreous structure, which can correspond to short ordering of ZnO₄ tetrahedra embedded in the glassy structure, see Ref. [34].
- d. Of the V1, V2, and V3 glasses containing Eu³⁺ ions, that with the highest content of CdO modifier helps in the formation of a crystalline phase of CdTe₂O₅ compound, see Ref. [35].

2.2.3. Photoacoustic spectra

The results of optical absorption, in the majority of cases, have pointed out that these glasses are transparent in the visible and near IR regions of the electromagnetic spectrum [37]. PA spectroscopy was employed in order to obtain more defined absorption spectra around the *edge absorption*.

PAS is the most direct method of obtaining the spectral dependence of the optical absorption coefficient in *edge absorption*. The absorption coefficient α is proportional to PA intensity, that is,

$$\alpha(h\nu) \propto \text{PA} \quad (15)$$

The PA spectrometer equipment often measures the quantity PA signal intensity versus α .

CdTeO₃ is a semiconductor of *direct band*, and the same is observed to the ZnO, CdO, and TeO₂ constituents of these glasses. Hence, near *edge absorption* spectral behavior follows [32]:

$$\alpha(h\nu) \propto (h\nu - E_g)^q \quad (16)$$

In this relation, α is the absorption coefficient, h is Planck's constant, ν is the frequency of the incident light, E_g is the optical energy measures in eV, and $q = 1/2$ for a *direct band*. Thus, of Eqs. (16) and (17), a measurement of $|\text{PA}|^2$ versus $h\nu$ typical plot for the E_g calculation [12].

In **Figure 17**, the PA spectra for the samples Yb127 and Yb136 are displayed, but Yb118 is not shown here. The E_g is estimated, its value was 3.47 eV for Yb136 and 3.6 eV for Yb127.

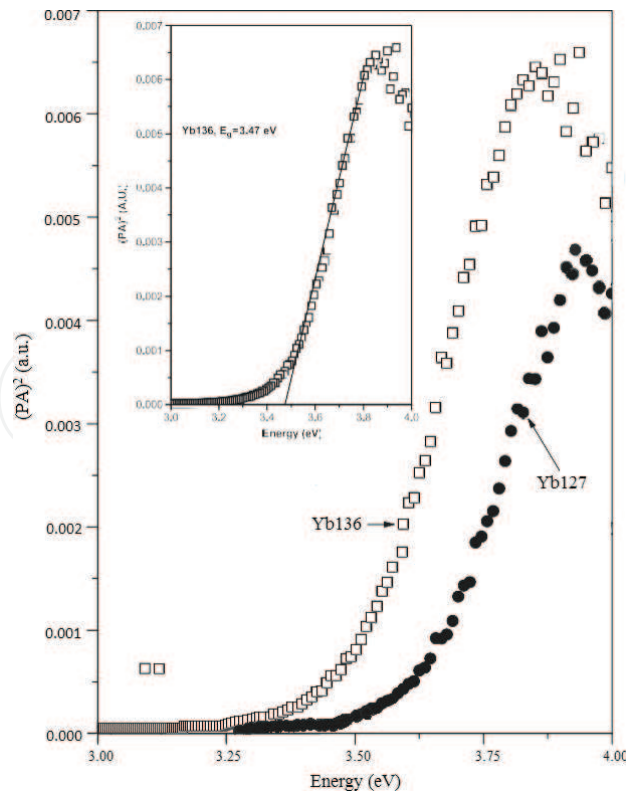


Figure 17. PA spectra of Yb127 and Yb136 glasses. In the inset, a typical plot used to determine E_g is illustrated.

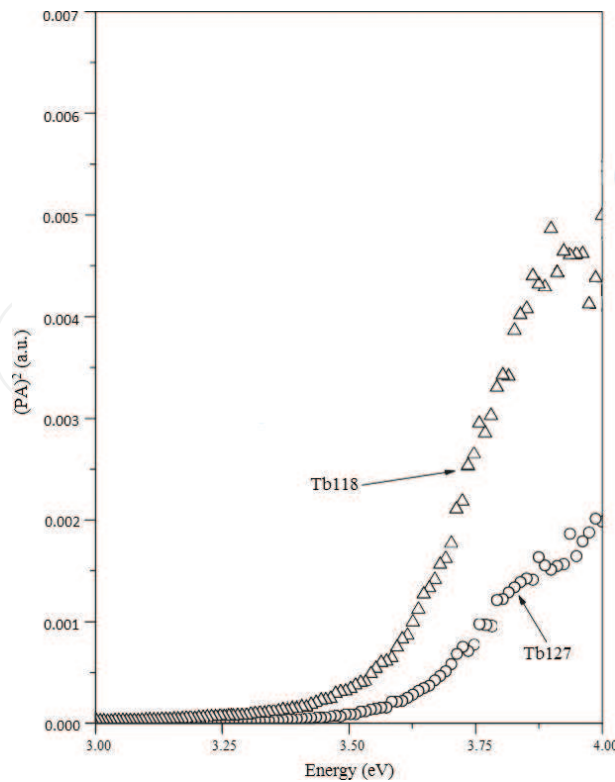


Figure 18. PA spectra of Tb118 and Tb127 glasses.

Figure 18 shows PA spectra for Tb118 and Tb127 glasses, but Tb136 is not displayed here. The E_g is estimated, its value was 3.51 eV for Tb118 and 3.6 eV for Tb127. In both cases, **Figures 17** and **18**, the value E_g is limited in the interval (3.47, 3.60) eV, which is very near of $E_g = 3.9$ eV, the bandgap of CdTeO_3 [32].

Figure 19 shows the PA spectra of the glasses doped with Nd^{3+} : V1, V2, and V3. By considering that one of the compounds in the tellurite matrix is ZnO, a material of direct bandgap (E_g) thus, a same value of $E_g = 3.45$ eV was calculated, for the three samples (see the inset of **Figure 19**, a plot to determine E_g). This value of E_g indicates a wide bandgap material, and was an expected result for this type of glass, but this value is lower than those reported for other glasses of the same matrix doped with other ions [34].

Now, the PA spectra for the V1, V2, and V3 glasses containing Eu^{3+} are exhibited in **Figure 20**. These spectra were acquired with steps of 1 nm/s, taking into account an average thickness of 1 mm. Obviously, this case is different from (a) to (c) cases because the crystalline phase of CdTe_2O_5 corresponds to a semiconductor more complex.

In the region between $\sim 10^1$ and $\sim 10^4 \text{ cm}^{-1}$, α obeys a simple relation,

$$\alpha \propto e^{(h\nu/E_0)} \quad (17)$$

which is termed the *Urbach tail*, being E_0 hardly depends on temperature [12]. In amorphous semiconductors, it is reported that E_0 varies linearly in the range of 0.05–0.1 eV. Using the *Urbach relation* and $\alpha(h\nu) \propto \text{PA}$, we obtain that

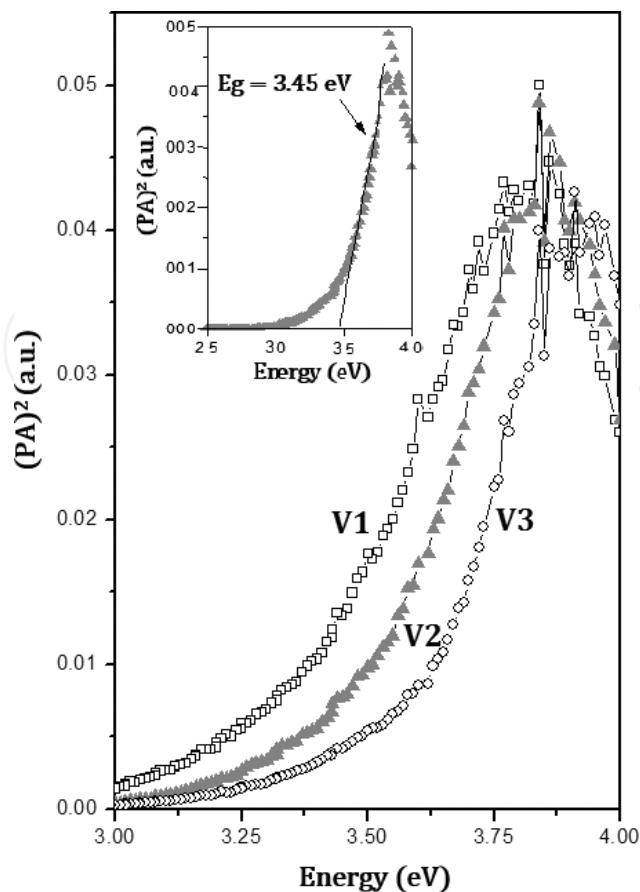


Figure 19. PA spectra of three glasses doped with Nd³⁺. In the inset, a typical plot used to determine E_g is illustrated, for the V2 glass.

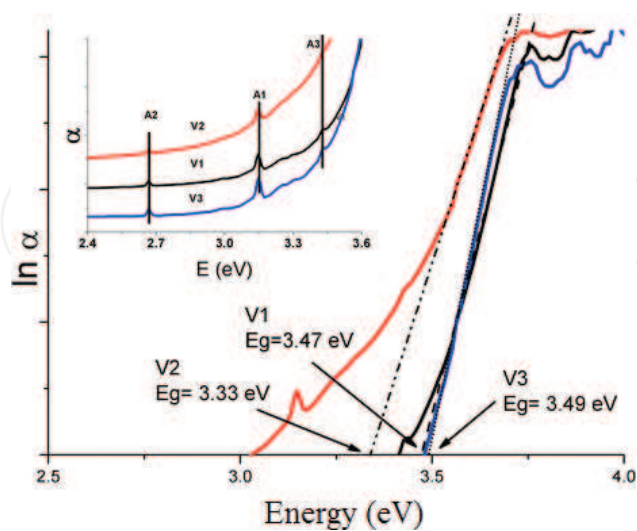


Figure 20. PA spectra of three glasses doped with Eu³⁺. In the inset, a typical plot used to determine E_g is illustrated.

$$\ln(\alpha) \propto h\nu \quad (18)$$

By applying Eq. (19), $\ln(\alpha)$ versus $h\nu$, for the V1–V3 glasses doped with europium, the energy of the optical absorption edge (E_g) was determined (see **Figure 20**). The obtained E_g values were 3.47, 3.33, and 3.49 eV for the V1, V2, and V3, respectively. The E_g for the starting oxides (ZnO, CdO, and TeO₂) is 3.3, 2.5, and 3.3 eV, respectively [35].

2.2.4. Photoluminescence spectra

Figure 21 shows the PL intensity of the samples Yb118, Yb127, and Yb136. Only the ${}^2F_{5/2} \rightarrow {}^2F_{7/2}$ transition was detected, as expected because this is the only transition reported until now for Yb-doped materials. The gradual diminution of the PL signal in the samples from Yb118 (the higher signal) until Yb136 (the lower signal) can be due to surface effects. This fact can be due to the difficulty to polish this kind of samples, in this way, some of them can present more roughness than others. The PL emissions of Yb-doped samples are accompanied by the second harmonic of the laser line (976 nm). The effects of the luminescence of the ion Yb³⁺ have already been observed in other hosts of tellurite glasses, showing a typical transition [38].

In **Figure 22**, the PL spectra for the samples Tb118, Tb127, and Tb136 are displayed. The signal of luminescence is very intense, with the emissions being identified as transitions between levels: ${}^5D_4 \rightarrow {}^7F_5$, ${}^5D_4 \rightarrow {}^7F_4$, ${}^5D_4 \rightarrow {}^7F_3$, of the ion Tb³⁺, respectively. It is important to stand out that some of the luminescent emissions were intense enough that could easily be seen with naked eye. As a matter of fact, the signal of three of the six samples at 548 nm (transition ${}^5D_4 \rightarrow {}^7F_5$) saturated our detector. On the other hand, it can be observed that it does not matter if the type of the matrix is crystalline or amorphous, since the position of the peaks does not change. PL in crystalline and amorphous matrices of RE-doped materials has already been reported in the literature.

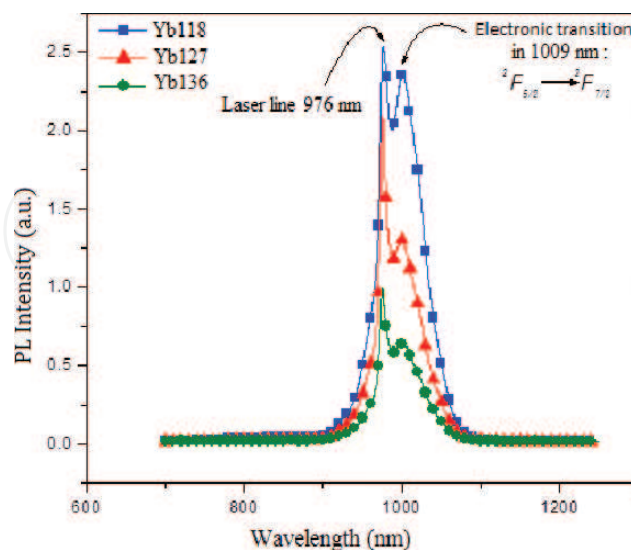


Figure 21. The photoluminescence []spectra of the Yb118, Yb127, and Yb136 samples are displayed.

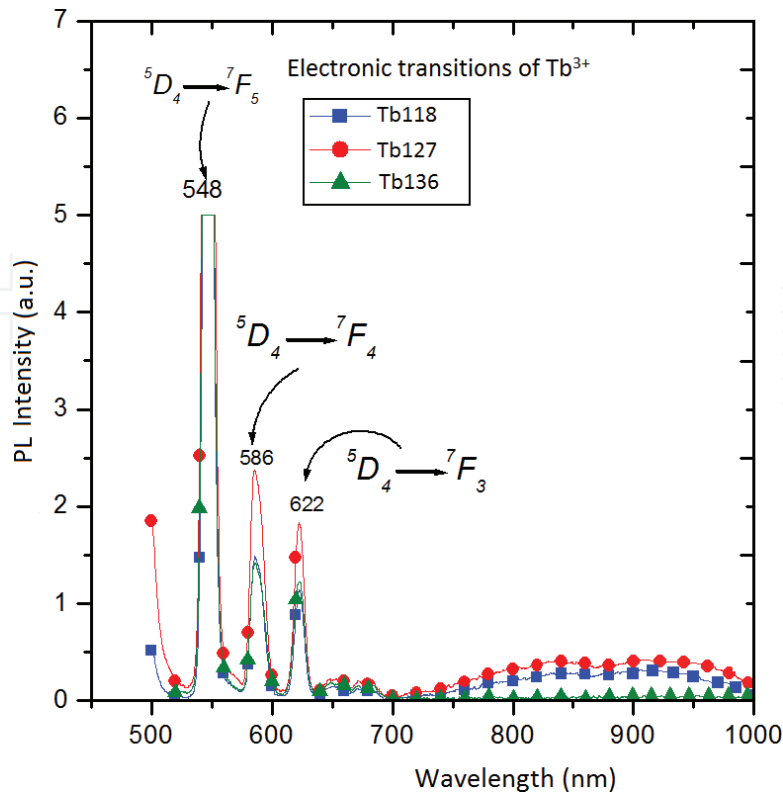


Figure 22. The photoluminescence spectra of the Tb118, Tb127, and Tb136 samples are displayed.

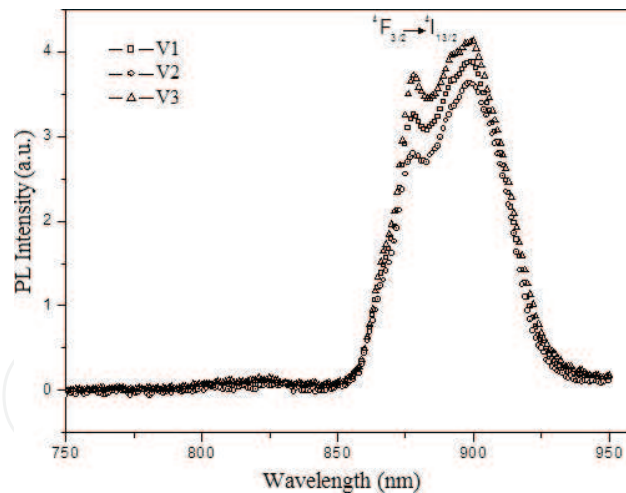


Figure 23. Photoluminescence spectra of V1, V2, and V3 glasses containing Nd³⁺.

PL spectra of glasses are shown in **Figure 23**, where only one transition $^4F_{3/2} \rightarrow ^4I_{9/2}$ appears due to the emission of the Nd³⁺ ions. Such a transition is typical in Nd³⁺-doped glasses and has also been reported by other authors [31].

PL spectra of glasses are shown in **Figure 24**, indicating the characteristic transitions due to the Eu³⁺ ion, which were identified as follows: $^5D_0 \rightarrow ^7F_1$, $^5D_0 \rightarrow ^7F_2$, $^5D_0 \rightarrow ^7F_3$, and $^5D_0 \rightarrow ^7F_4$, which appear around 590, 620, 650, and 700 nm, respectively. Such transitions are typical in

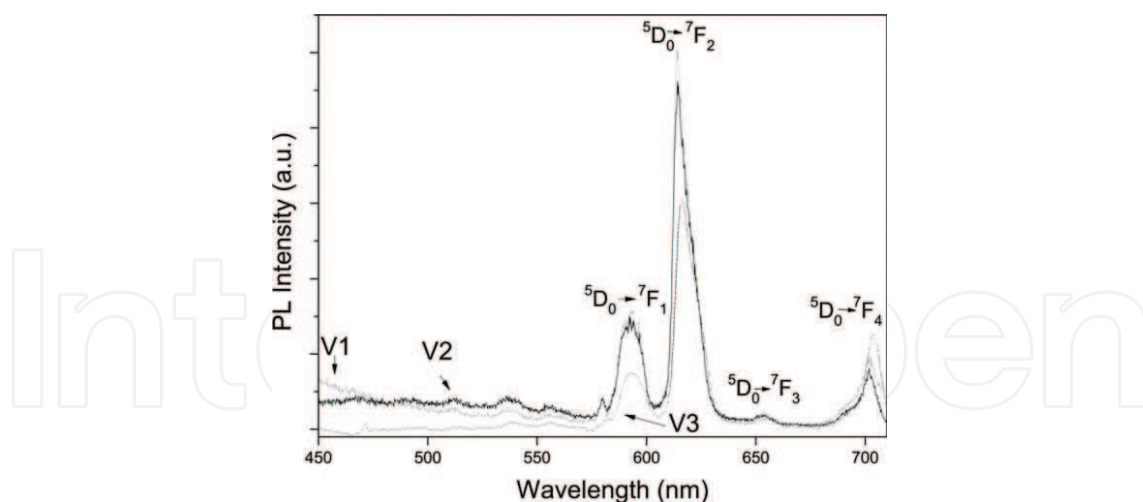


Figure 24. Photoluminescence spectra of V1, V2, and V3 glasses containing Eu^{3+} .

Eu^{3+} -doped-glasses and have also been reported previously in glasses containing this dopant [39, 40]. The emission spectra for the three samples are dominated by the ${}^5D_0 \rightarrow {}^7F_2$ transition, the highest intensity, indicating that Eu^{3+} occupies a low symmetry site. The intensity ratio of $R = I({}^5D_0 \rightarrow {}^7F_2)/I({}^5D_0 \rightarrow {}^7F_1)$, which is a measure of Eu^{3+} ion site symmetry, is calculated to be upper to the unit. This result is an indication that Eu^{3+} ions occupy mainly the lattice site of noninversion symmetry [1].

3. Conclusions

1. For NaCl crystals containing a considerable concentration of Eu^{2+} ions (≈ 200 ppm or 0.1 wt%), the following results were confirmed:
 - 1.1 The decay curve of the luminescent intensity due to Eu^{2+} ions had an approximately exponential behavior.
 - 1.2 Luminescent emission spectra consist of a single broadband centered approximately between 430 and 450 nm, which is typical of Eu^{2+} ions in crystalline matrices mainly alkali halides.
2. Glasses of the ZnO-CdO-TeO_2 system were doped with Yb^{3+} , Tb^{3+} , Nd^{3+} , or Eu^{3+} ions:
 - 2.1 Optical absorption spectra showed that these glasses are transparent in much of the optical region of the electromagnetic spectrum.
 - 2.2 The photoluminescent emissions of these glasses investigated were assigned to typical transitions of those rare earth ions that already have been identified in other systems vitreous.
 - 2.3 The results seen in the photoacoustic spectra, and their correlation with XRD patterns, have allowed to obtain the bandwidth of optical energy (optical bandgap) of

crystalline phases that are embedded in the vitreous structure characteristic of the material under study.

- 2.4 PA spectroscopy allows to determine the optical energy gap values that were found with those reported in other systems already studied by this technique.
- 2.5 Tellurite glasses containing Yb^{3+} are potential candidates for parent, a single line of excitation laser ${}^2F_{7/2} \rightarrow {}^2F_{5/2}$.
- 2.6 Of the glasses containing CdTeO_3 , crystals can be used in the technology of devices semiconductor, and also may be applied to nanotechnology.

Acknowledgements

The authors thank Geologist Rojas Santiago, Department of Geology, University of Sonora, for his technical help in this chapter. The authors also thank Mechatronic Engineer Tadeo R. Marielvis J., Department of Industrial Engineering, University of Sonora, for her technical help in this chapter.

f_{13}^1, f	2F			
f_{12}^2, f	${}^1S, {}^1D, {}^1G, {}^1I$	${}^3P, {}^3F, {}^3H$		
f_{11}^3, f	${}^2P, {}^2D, {}^2F, {}^2G, {}^2H, {}^2I, {}^2K, {}^2L$	${}^4S, {}^4D, {}^4F, {}^4G, {}^4I$		
f_{10}^4, f	${}^1S, {}^1D, {}^1F, {}^1G, {}^1H, {}^1I, {}^1K, {}^1L, {}^1N$	${}^3P, {}^3D, {}^3F, {}^3G, {}^3H, {}^3I, {}^3K, {}^3L, {}^3M$	${}^5S, {}^5D, {}^5F, {}^5G, {}^5I$	
f^5, f^9	${}^2P, {}^2D, {}^2F, {}^2G, {}^2H, {}^2K, {}^2L, {}^2M, {}^2N, {}^2O$	${}^4S, {}^4P, {}^4D, {}^4F, {}^4G, {}^4H, {}^4I, {}^4K, {}^4L, {}^4M$	${}^6P, {}^6F, {}^6H$	
f^6, f^8	${}^1S, {}^1P, {}^1D, {}^1F, {}^1G, {}^1H, {}^1I, {}^1K, {}^1L, {}^1M, {}^1N, {}^1Q$	${}^3P, {}^3D, {}^3F, {}^3G, {}^3H, {}^3I, {}^3K, {}^3L, {}^3M, {}^3N, {}^3O$	${}^5S, {}^5P, {}^5D, {}^5F, {}^5G, {}^5H, {}^5I, {}^5K, {}^5L$	7F
f^7	${}^2S, {}^2P, {}^2D, {}^2F, {}^2G, {}^2H, {}^2I, {}^2K, {}^2L, {}^2M, {}^2N, {}^2O, {}^2Q$	${}^4S, {}^4P, {}^4D, {}^4F, {}^4G, {}^4H, {}^4I, {}^4K, {}^4L, {}^4M, {}^4N$	${}^6P, {}^6D, {}^6F, {}^6G, {}^6H, {}^6I$	8S

Appendix 1. Table of terms corresponding to the 4f n electron configurations.

Author details

Carlos Ruvalcaba Cornejo

Address all correspondence to: carlruval@yahoo.com.mx

University of Sonora, Hermosillo, Sonora, Mexico

References

- [1] Blasse G. and Grabmaier B.C. *Luminescent Materials*. Berlin: Springer-Verlag; 1994. 232 p.
- [2] Ropp R.C. *Luminescence and the Solid State*. 2nd ed. Amsterdam: Elsevier; 1991. 711 p.
- [3] Jorgensen C.K., Reisfeld, R. *Chemistry and spectroscopy of the rare earths*. *Topics in Current Chemistry*. 1982; **100**:127–167.
- [4] Stevens K.W.H. *Magnetic Ions in Crystals*. NJ: Princeton University Press; 1997. 249 p.
- [5] Sobelman I.I. *Atomic Spectra and Radiative Transitions*. Berlin Heidelberg: Springer-Verlag; 1994. DOI: 10.1007/978-3-662-05905-0
- [6] Cohen-Gannoudji C., Diu B., Laloe F. *Quantum Mechanics*. New York, NY: Wiley-VCH; 1991. 640 p.
- [7] Di Bartolo B. *Optical Interactions in Solids*. Cambridge, MA: John Wiley & Sons; 1968. 541 p.
- [8] Hüfner S. *Optical Spectra of Transparent Rare Earth Compounds*. New York, NY: Academic Press; 1978. 237 p.
- [9] López F.J., Murrieta S.H., Hernández A.J., Rubio O.J. Optical absorption and luminescence investigations of the precipitated phases of Eu in NaCl and KCl single crystals. *Physical Review B*. 1980; **22**:6428. DOI: <http://dx.doi.org/10.1103/PhysRevB.22.6428>
- [10] Ruvalcaba-Cornejo C. Master's Thesis. 2002. Pages 30–32. Effect of the symmetry of crystalline field on Eu²⁺ ions in NaCl crystals [Master's thesis]. Hermosillo, Sonora: University of Sonora; 2002. 46 p.
- [11] Manasresh M.O., Jiang H.X. *III-Nitride Semiconductors: Optical Properties I*. Great Britain: Taylor & Francis Books; 2002. 417 p.
- [12] Mandelis A. *Photoacoustic and Thermal Wave Phenomena in Semiconductors*. 1st ed. Toronto, Canada: Elsevier Science Publishing; 1987. 480 p.
- [13] Rosencwaig A. *Photoacoustic and Photoacoustic Spectroscopy*. New York, NY: John Wiley & Sons; 1987.
- [14] Zarzycki J. *Glasses and the Vitreous State*. Great Britain: Cambridge University Press; 1991. 505 p.
- [15] Fernandez J.M. *The Glass (University texts)*. Madrid: High Council for Scientific Research; 1991.
- [16] D'Amore F., Di Giulio M., Pietralunga S.M., Zappettini A., Nasi L., Rigato V., Martinelli M. Sputtered stoichiometric TeO₂ glass films: Dispersion of linear and nonlinear optical properties. *Journal of Applied Physics*. 2003;**94**(3):1654.
- [17] Mirgorodsky A.P., Merle-Méjean T., Champarnaud J.C., Thomas P., Frit B. Dynamics and structure of TeO₂ polymorphs: model treatment of paratellurite and tellurite; Raman

- scattering evidence for new γ - and δ -phases. *Journal of Physics and Chemistry of Solids*. 2000;**61**(4):501–509. DOI: 10.1016/S0022-3697(99)00263-2
- [18] Dimitriev Y., Dimitrov V., Gattef E., Kashchieva E and Petkov H. Effect of the mode formation on the structure of tellurite glasses. *Journal of Non-Crystalline Solids*. 1987;**95**:937–944. DOI: 10.1016/S0022-3093(87)80701-9
- [19] Petkov V., Stachs O., Gerber Th., Ilieva D. and Dimitriev Y. Atomic ordering in $x\text{Ga}_2\text{O}_3 \cdot (100-x)\text{TeO}_2$ glasses ($x=10, 17.5, 25$) by X-ray diffraction. *Journal of Non-Crystalline Solids*. 1999;**248**(1):65–74. DOI: 10.1016/S0022-3093(99)00091-5
- [20] Zwanziger J.W. Structure and chemical modification in oxide glasses. *International Reviews in Physical Chemistry*. 1998; **17**(1):65–90.
- [21] Hoppe U., Yousef E., Rüssel C., Neuefeind J. and Hannon A. C. Structure of zinc and niobium tellurite glasses by neutron and x-ray diffraction. *Journal of Physics: Condensed Matter*. 2004; **16**(9):1645–1663. DOI: 10.1088/0953-8984/16/9/013
- [22] Doremus R.H. *Glass Science*. 2nd ed. New York, NY: John Wiley & Sons; 1994. 339 p.
- [23] Muñoz J.E. Extinction of the Luminescence of Eu^{2+} on Alkaline Halides Induced by Precipitation [PH thesis]. Madrid: Autonomous University of Madrid; 1991.
- [24] Wang J.S., Vogel E.M., Snitzer E., Jackel J.L., Da Silva V.L., Silberberg Y., et al. 1.3 μm emission of neodymium and praseodymium in tellurite-based glasses. *Journal of Non-Crystalline Solids*. 1994;**178**:109–113
- [25] Miyajima T., Tojyo T., Asano T., Yanashima K., Kijima S., Hino T., et al. GaN-based blue laser diodes. *Journal of Physics: Condensed Matter*. 2001;**13**(32):7099.
- [26] Bey H. J. Light-Emitting Diodes-Photolithography Patterns Plastic LEDs. *Laser Focus World*. 1997; **33**:36.
- [27] Lenth W., Macfarlane R.M. Upconversion lasers. *Optics & Photonics News*. 1992;**3**(3):8.
- [28] Ozen G., Demirata B., Ovecoglu M.L., Genc A. Thermal and optical properties of Tm^{3+} doped tellurite glasses. *Spectrochimica Acta Part A: Molecular and Biomolecular Spectroscopy*. 2001;**57**(2):273.
- [29] Kim S.H., Yoko T. Nonlinear optical properties of TeO_2 - based glasses: $\text{MO}_x\text{-TeO}_2$ ($M=\text{Sc}, \text{Ti}, \text{V}, \text{Nb}, \text{Mo}, \text{Ta}, \text{and W}$) binary glasses. *Journal of the American Ceramic Society*. 1995;**78**(4):1061. DOI: 10.1111/j.1151-2916.1995.tb08437.x
- [30] Rakov N., Maciel G.S., Sundheimer M.L., Menezes L. de S., Gomes A.S.L., Messaddeq Y., et al. Blue upconversion enhancement by a factor of 200 in Tm^{3+} -doped tellurite glass by codoping with Nd^{3+} ions. *Journal of Applied Physics*. 2002;**92**(10):6337.
- [31] D.L. Sidebottom, M.A. Hruschka, B.G. Potter, R.K. Brow. Increased radiative lifetime of rare earth-doped zinc oxyhalide tellurite glasses. *Applied Physics Letters*. 1997;**71**(14):1963–1965.

- [32] Ruvalcaba-Cornejo C., Flores-Acosta M., Zayas Ma. E., Lozada-Morales R., Palomino-Merino R., Espinosa J.E., et al. Photoluminescence properties of the ZnO-CdO-TeO₂ system doped with the Tb³⁺ and Yb³⁺ ions. *Journal of Luminescence*. 2008;**128**:213. DOI: 10.1016/j.jlumin.2007.07.004
- [33] Rubalcava-Cornejo C., Zayas Ma. E., Castillo S.J., Palafox J.J., Lozada-Morales R., and Rincón J. Ma. Structural properties of rare earth doped ZnO-CdO-TeO₂ system. *Journal of Glass Science Technology. B*. 2009;**50**(1):19–22.
- [34] Ruvalcaba-Cornejo C., Zayas Ma. E., Castillo S.J., Lozada-Morales R., Pérez-Tello M., Díaz C.G., et al. Optical and thermal analysis of ZnO-CdO-TeO₂ glasses doped with Nd³⁺. *Optical Materials*. 2011;**33**:823–826. DOI: 10.1016/j.optmat.2011.01.001.
- [35] Ruvalcaba-Cornejo C., Zayas Ma. E., Lozada-Morales R., Rincón J. Ma. and De L. Flores A. Effect of the Eu³⁺ addition on photoluminescence and microstructure of ZnO-CdO-TeO₂ glasses. *Journal of the American Ceramic Society*. 2013;**96**:3084–3088. DOI:10.1111/jace.12542
- [36] Zayas M.E., Arizpe H., Castillo S.J., Medrano F., Diaz G.C., Rincón J.M., et al. Glass formation area and structure of glassy materials obtained from the ZnO-CdO-TeO₂ ternary system. *Physics and Chemistry of Glasses*. 2005;**46**(1):46–57.
- [37] Ruvalcaba C.C. Optical and Structural Study of Rare Earth Ions Doped Glasses of the ZnO-CdO-TeO₂ System [PH thesis]. University of Sonora: Department of Research in Polymers and Materials; 2009. 90 p.
- [38] M. Dejneka, E. Snitzer, R.E. Riman. Blue, green and red fluorescence and energy transfer of Eu³⁺ in fluoride glasses. *Journal of Luminescence*. 1995;**65**(5):227–245. DOI: 10.1016/0022-2313(95)00073-9
- [39] J. Ozdanova, H. Ticha, L. Tichy, Optical gap and Raman spectra in some (Bi₂O₃)_x(WO₃)_y(TeO₂)_{100-xy} and (PbO)_x(WO₃)_y(TeO₂)_{100-xy} glasses. *Journal of Non-Crystalline Solids*. 2009;**355**:2318–2322.
- [40] Hongpeng Y., Masayuki N. Three-photon-excited fluorescence of Al₂O₃-SiO₂ glass containing Eu³⁺ ions by femtosecond laser irradiation. *Applied Physics Letters*. 2004;**84**.

